Materials Research. 2016; 19(4): 802-806
DOI: http://dx.doi.org/10.1590/1980-5373-MR-2015-0536

Microstructure and Properties of Coating of FeAlCuCrCoMn High Entropy Alloy Deposited by Direct Current Magnetron Sputtering

Xiaochun Li[a], Zuoyun Zheng[b], Dan Dou[b], Jianchen Li[b]*

[a]Engineering Training Centre, Jilin University, Changchun, 130025, China
[b]Key Laboratory of Automobile Materials, Ministry of Education and School of Materials Science and Engineering, Jilin University, Changchun, 130025, China

Received: September 8, 2015; Revised: December 22, 2015; Accepted: May 10, 2016

The coatings of FeAlCuCrCoMn high entropy alloy were deposited by direct current magnetron sputtering. The microstructure and the mechanical and corrosion properties of the coatings are investigated. A perfect dense and smooth coating could be obtained. The coatings exhibit single FCC solid solution as increasing deposited time. The thickness of the coatings increases with the increasing deposited time, the biggest thicknesses is 1.788 µm. The hardness and Young's modulus of the coatings are 17.5 and 186 GPa, respectively. All coatings exhibit better corrosion resistance than the 201 stainless steel in acidic alkali and salt corrosion mediums.

Keywords: *High entropy alloy, coating, microstructure, properties, magnetron sputtering*

1. Introduction

The conventional alloys generally consist of one principal element associated with a substantial amount of other elements to enhance the properties and processing[1], which differ from the high-entropy alloy (HEA) recently proposed by Yeh *et al.* [2,3]. HEA is a novel concept for the alloy system that has multiple principal elements with equimolar or near-equimolar ratios in the rang of 5-35 at.%. When all elements in the alloys have an equal atomic percentage, the configurational entropy of the liquid alloy S^l_f will reach its maximum of, $S^l_f = -R\sum_{i=1}^{i=N} x_i \ln x_i$ where x_i is the concentration of component *i,* and *N* denotes the number of principal components, *R* the ideal gas constant, and superscript *l* denotes the liquid. At $N = 5$, $S^l_m = 1.61R$; which is larger than the corresponding melting entropy S_m of metallic elements with usual values of 1.1-1.3*R*. Due to the high entropy characteristics, this kind of alloys is named as the high-entropy alloys (HEA). If the value of the formation enthalpy for an intermetallic compound H^c is comparable with the size of TS^l_f where *T* is the absolute temperature, and the cooling rate is big enough, a disordered solid solution could be present. During the formation of the solid solution, the atoms in the liquid need only minor movement being smaller than atomic radius *r*. Thus, the formation barrier is small [4]. In addition, a large value of the configurational entropy of the solid solution $S^s_f \approx S^l_f$ exists, which stabilizes the solid solution, where the superscript *s* denotes the solid solution. Note that the solid solution here means that its structure is the same of the structure of a marginal component and all components are located freely at any site in the lattice. Due to the solution hardening effect, the HEA with high hardness offer potential industrial applications, such as tools, molds, dies, high temperature parts where high strength, good wear and oxidation resistances are required. HEA could be obtained by rapid solidification, mechanical alloying, chemical vapor deposition (CVD), physical vapor deposition (PVD) or direct current magnetron sputtering (DCMS) methods.

In recent years, HEA films have been widely studied, such as TiVCrZrHf film[5], AlCrMoTaTiZr film[6,7], etc. Moreover, HEA coatings have been proposed for the potential applications as protective films[8-10], wear-resistant materials[11], corrosion-resistant materials[12], and coatings in communication devices[13]. That is due to their interesting properties, such as high hardness[14], strength[15,16], wear resistance[17,18], and microstructure stability against heat treatment[19-21].

In previous work[22,23], we have developed the novel HEA alloys (i.e. FeCoNiCu system) with a single FCC crystalline structure, which exhibits good plastic properties with the tensile strain up to 18%. Musil et al. reported the hard and super-hard Zr-Ni-N nanocomposite films with the hardness of 40 GPa[24]. The similar strengthening effect was also revealed in VN[25]. Moreover, the addition of other element, such as Al, was found to further improve the thermal stability of the film[26,27]. Based on the above observations, the multicomponent FeAlCuCrCoMn film is expected to possess excellent mechanical properties.

In this contribution, the coatings of FeAlCuCrCoMn HEA are prepared by using direct current magnetron sputtering system at a low depositing temperature. In addition, the microstructure, hardness and Young' modulus and electrochemical corrosion of the coatings were systematically investigated and discussed.

2. Experimental methods

The FeAlCuCrCoMn HEA was melted for at least 5 times by the arc melting-method under a purified argon gas atmosphere. Then, it was shaped into a disc of 60 mm in diameter and 5 mm in thickness as a target. Table 1 lists the composition of the target and the atomic ratios of each element measured by energy dispersive spectrometry (EDS). Quartz glass wafers were cleaned sequentially in de-ionized (DI)

* e-mail: ljc@jlu.edu.cn

Table 1: Composition of the FeAlCuCrCoMn high-entropy alloy target (at.%)

Element	Fe	Co	Ni	Cu	V	Zr	Al
Nominal composition	14.28	14.28	14.28	14.28	14.28	14.28	14.28
Composition By EDS	13.96	13.95	13.20	13.83	14.57	15.19	15.31

water, acetone and DI water, for the following deposition of the coatings of FeAlCuCrCoMn by DC magnetron sputtering in a mixture atmosphere of Ar, the coatings were deposited under a plasma power of 80-150 W, a constant working pressure of 0.9 Pa, the distance between the substrate and the target was set as 75 mm.

The phase structure analysis of the target and the coatings was performed on Rigaku D/max 2500 X-ray diffractometer at 50 KV and 250 mA (XRD, D/Max 2500pc) with the scanning angles ranging from 20 to 90 degree at a scanning rate of 2 degree/min. Both the surface morphology and thickness of the deposited coatings were observed by field-emission scanning electron microscopy (FESEM, JEOL JSM 6700F). The chemical compositions of the coatings were analyzed by EDS. The hardness and Young's modulus of the coatings were measured by a nanoindenter (XP nanomechanical testing system, MTS Corporation), during which the penetration depth of the indenter was controlled at about 1/10 of the film thickness to avoid substrate effect.

The electrochemical measurement was performed on a V3 Microcomputer-based Electrochemical System, which was controlled by a computer and supported by self-designed software. Electrochemical tests were carried out in 3.5 % NaCl solution, 5% NaOH solution and 10% H_2SO_4 solution respectively using a classic three-electrode cell with a platinum plate (Pt) as counterelectrode and a Ag/AgCl electrode (+207 mV vs. SHE) as reference. Before testing, the working electrode was cleaned in acetone agitated ultrasonically for 10 min. The exposed area for testing was obtained by doubly coating with epoxy resin (EP 651), leaving an uncovered area of approximately 1 cm^2. During the potentiodynamic sweep experiments, the samples were first immersed into the solution for about 20 min to stabilize the open circuit potential E_0. Subsequently, the potentiodynamic curves were recorded by sweeping the electrode potential at a sweeping rate of 5 mV/s. The log(i)–E curves were measured after the above electrochemical measurements. The corrosion potential E_{corr} and corrosion current density i_{corr} were deduced from these log(i)–E curves by using the CorrView software.

3. Results and discussion

Figure 1 shows the X-ray diffraction curve of the target of FeAlCuCrCoMn HEA. As indicated, the crystalline structures are composed of α (cubic) phase with the space group of Fm3m (225). Figure 2 illustrates X-ray diffraction curves of the coatings of FeAlCuCrCoMn alloy at different deposited times under 100W deposited power. It can be clearly seen that the coatings exhibit amorphous structure at short deposited time, dramatically different from that of the as-melted HEA target shown in Figure 1. This phenomenon was also observed in the preparation of the coatings of

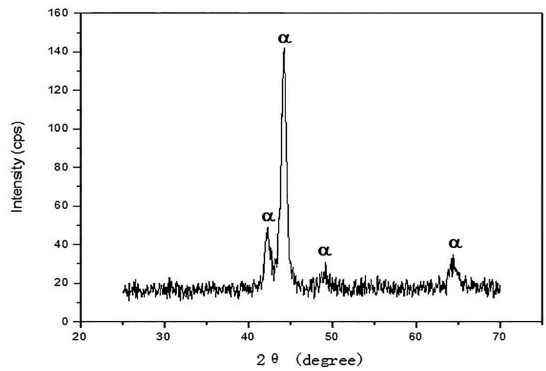

Figure 1: X-Ray diffraction curve of the FeAlCuCrCoMn target.

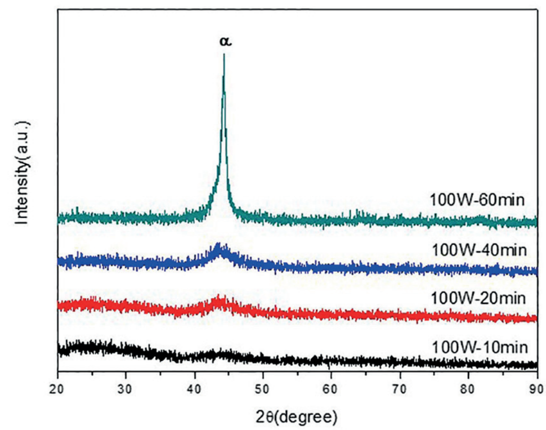

Figure 2: X-Ray diffraction curves of the coatings at different time under 100W plasma power.

the AlCrSiTiV[28], AlFeCoNiCuZrV[29,30], and AlMoNbSiTaTiVZr[31], the films of $AlCoCrCu_{0.5}NiFe$[32] and AlCrTaTiZr HEA[33]. The reason that the deposited HEA films were in amorphous state can be explained by the rules proposed by Inoue[34], in which the glass-forming ability can be strengthened for multicomponent systems. When deposited time increase further, the structure of the coatings of FeAlCuCrCoMn alloy is single FCC solid solution. When the film is very thin after a short time of deposition, the structure of film is controlled by the substrate, so that film is amorphous similar to the substrate (quartz glass wafers), while the thickness of the film increases to a certain extent, the influence of substrate on film becomes less, hence the film transforms into FCC solid solution structure like the bulk alloy. Figure 3 is XRD patterns of the coatings of FeAlCuCrCoMn alloy under different deposited power at 60 minutes. The results show that the coatings all exhibit single FCC structure.

Figure 4 - Figure 6 show the top-view FESEM images of the FeAlCuCrCoMn coatings deposited at different deposited time under definite plasma power, illustrating the evolution of morphology. It can be see that the coatings are composed of nanoparticles with different geometric morphology as time changes. When time is short, the size of the nanoparticles is less than 10 nm under 80 W plasma power, but the nanoparticles occur gather together with increasing time, and the coating becomes no integrated. For high deposited power, the surface of the coating becomes smoother and forms a smooth coating

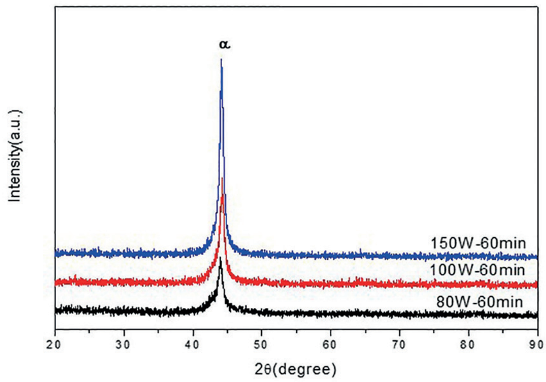

Figure 3: X-Ray diffraction curves of the coatings under different plasma power at 60 minutes.

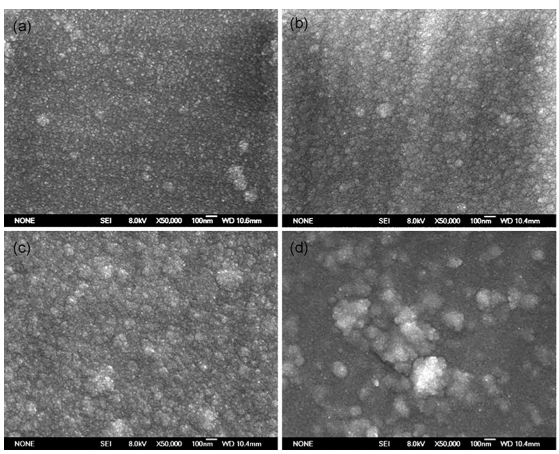

Figure 4: FESEM morphology of the coatings at different times under 80W plasma power. (a) 10 minutes, (b) 20 minutes, (c) 40 minutes, (d) 60 minutes.

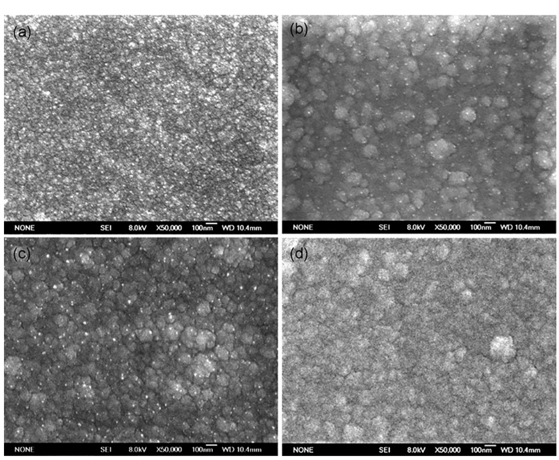

Figure 5: FESEM morphology of the coatings at different times under 100W plasma power. (a) 10 minutes, (b) 20 minutes, (c) 40 minutes, (d) 60 minutes.

and the size of the particles increases with increasing time, a perfect dense coating can be obtained. However, when the power is 150 W, the particles coarsening obviously, and the dense coating seems to be destructed, the coating surfaces

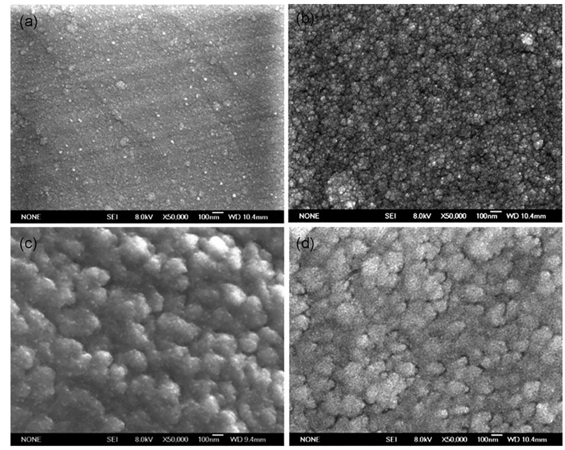

Figure 6: FESEM morphology of the coatings at different times under 150W plasma power. (a) 10 minutes, (b) 20 minutes, (c) 40 minutes, (d) 60 minutes.

become looser and have more micro-holes. Figure 7 show that the thicknesses of the coatings increase with the increasing the time, but the increasing of thickness is slowdown with further increasing of time. It is reason that a spot of oxide film easily formed on the target surface during sputtering due to the good affinity of all the target elements with oxygen, hindering the atoms from sputtering, which is a typical result of target poisoning[35]. The largest thicknesses can reach 1.788 μm.

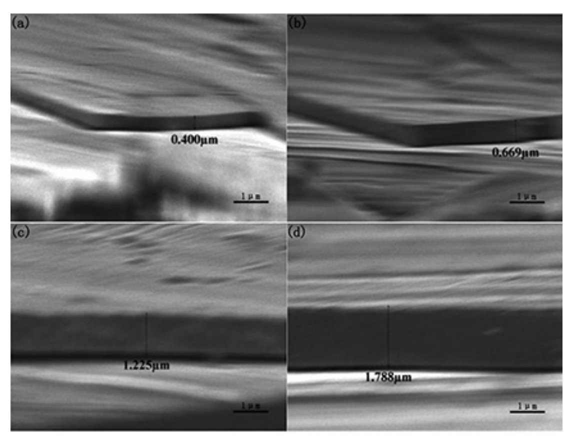

Figure 7: Thickness of the coatings at different time under 100 W plasma power. (a) 10 min, (b) 20 min, (c) 40 min, (d) 60 min.

Figure 8 plots the hardness and Young's modulus of the FeAlCuCrCoMn coatings. The results show that the hardness and Young's modulus of the coatings increase with increasing deposited time, and reach maximum values of 17.5 and 186 GPa, respectively. They are relatively superior to typical coatings of pure metals and alloys, which is mainly caused by the great solid-solution strengthening effect from the addition of a large amount of different-size atoms, and might be due to the perfect dense and smooth.

Figure 9 is the potentiodynamic polarization behaviour of the coatings and 201 stainless steel in sodium chloride, sodium hydroxide solution and sulfuric acid solution respectively. Table 2 is the electrochemical parameters associated with

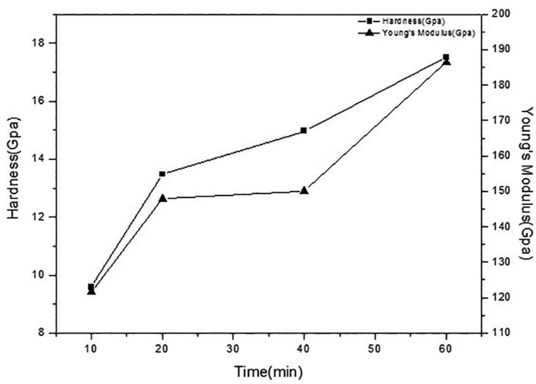

Figure 8: Hardness and Young's Modulus of the coatings at different time under 100 W plasma power.

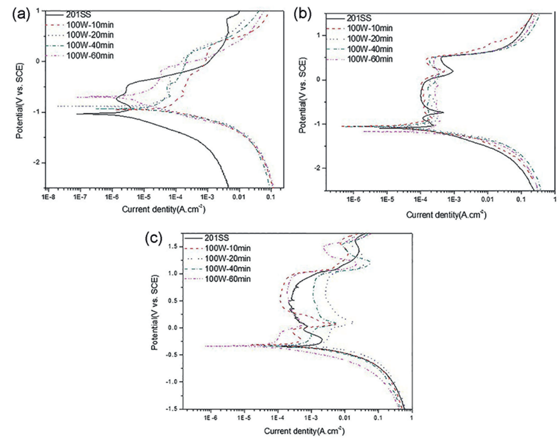

Figure 9: The potentiodynamic polarization curves of the coatings in different corrosion mediums. (a) 3.5 NaCl, (b) 5% NaOH, (c) 10% H_2SO_4.

Table 2: The electrochemical parameters of the coatings in different corrosion mediums respectively

	3.5% NaCl		5% NaOH		10% H2SO4	
	E_{crro} (mV)	i_{crro} (μAcm^{-2})	E_{crro} (mV)	i_{crro} (μAcm^{-2})	E_{crro} (mV)	i_{crro} (μAcm^{-2})
201SS	-948.62	86.627	-1092.4	355.11	-348.25	2836.8
100W-10 minutes	-934.43	17.425	-1050.1	15.123	-312.34	358.54
100W-20 minutes	-821.05	14.839	-1071.7	7.7652	-319.99	552.52
100W-40 minutes	-883.93	12.912	-1054.6	34.594	-336.41	871.83
100W-60 minutes	-702.33	2.6651	-1169.7	149.97	-333.93	742.55

the general corrosion behaviour of the coatings in different corrosion mediums respectively. The results show that the FeAlCuCrCoMn coatings have a wider passive region in these corrosion mediums, which indicates a tendency of the coatings to passivate. This superior corrosion resistance of the coatings of HEA may be attributed to the fact that there are fine grain and no segregation.

4. Conclusion

The coatings of FeAlCuCrCoMn high-entropy alloy have been deposited successfully using direct current magnetron sputtering. The coatings exhibit amorphous structure for short deposited time, dramatically different from the as-melted HEA target. The coatings exhibit single FCC solid solution as increasing deposited time. The thickness of the coatings increases with the increasing deposited time, the biggest thicknesses is 1.788 μm. a perfect dense and smooth FCC solid solution coating is obtained with the hardness and Young's modulus up to the maximum values of 17.5 and 186 GPa, respectively. All coatings exhibit better corrosion resistance than the 201 stainless steel in acidic alkali and salt corrosion mediums.

5. Acknowledgements

The authors gratefully acknowledge the financial supports from NNSFC (Grant No. 50571040), National Key Basic Research and Development Program (Grant No.2014CB643306) and National Foundation of Doctoral Station (Grant No. 20100061110019).

6. References

1. Handbook Committee. *Metals Handbook*, vol. 1, 10th ed. Materials Park: ASM International; 1990. p.945-949.
2. Yeh JW, Chen SK, Lin SJ, Gan JY, Chin TS, Shun TT, et al. Nanostructured High-Entropy Alloys with Multiple Principal Elements: Novel Alloy Design Concepts and Outcomes. *Advanced Engineering Materials*. 2004;6(5):299-303.
3. Huang PK, Yeh JW, Shen TT, Chen SK. Multi-Principal-Element Alloys with Improved Oxidation and Wear Resistance for Thermal Spray Coating. *Advanced Engineering Materials*. 2004;6(1-2):74-78.
4. Pan JS, Tong JM, Tian MB. *Fundamentals of materials science*. Beijing: Tsinghua University Press; 1998. p.83-90.
5. Liang SC, Tsai DC, Chang ZC, Sung HS, Lin YC, Yeh YJ, et al. Structural and mechanical properties of multi-element (TiVCrZrHf)N coatings by reactive magnetron sputtering. *Applied Surface Science*. 2011;258(1):399-403.
6. Cheng KH, Lai CH, Lin SJ, Yeh JW. Structural and mechanical properties of multi-element $(AlCrMoTaTiZr)N_x$ coatings by reactive magnetron sputtering. *Thin Solid Films*. 2011;519(10):3185-3190.
7. Liang SC, Chang ZC, Tsai DC, Lin YC, Sung HS, Deng MJ, et al. Effects of substrate temperature on the structure and mechanical properties of (TiVCrZrHf)N coatings. *Applied Surface Science*. 2011;257(17):7709-7713.

8. Tsai MH, Yeh JW, Gan JY. Diffusion barrier properties of AlMoNbSiTaTiVZr high-entropy alloy layer between copper and silicon. *Thin Solid Films*. 2008;516(16):5527-5530.

9. Chen TK, Shun TT, Yeh JW, Wong MS. Nanostructured nitride films of multi-element high-entropy alloys by reactive DC sputtering. *Surface and Coatings Technology.* 2004;188-189:193-200.

10. Chang SY, Chen DS. (AlCrTaTiZr)N/(AlCrTaTiZr)N-0.7 bilayer structure of high resistance to the interdiffusion of Cu and Si at 900 degrees C. *Materials Chemistry and Physics*. 2011;125(1):5-8.

11. Ren B, Liu ZX, Shi L, Cai B, Wang MX. Structure and properties of $(AlCrMnMoNiZrB_{0.1})N_x$ coatings prepared by reactive DC sputtering. *Applied Surface Science*. 2011;257(16):7172-7178.

12. Chen YY, Duval T, Hung UD, Yeh JW, Shih HC. Microstructure and electrochemical properties of high entropy alloys—a comparison with type-304 stainless steel. *Corrosion Science*. 2005;47(9):2257-2279.

13. Chen HK, Li SH, Duh JG. Structure and soft magnetic properties of Fe-Co-Ni-based multicomponent thin films. *Journal of Electronic Materials*. 2005;34(12):1480-1483.

14. Zhou YJ, Zhang Y, Wang YL, Chen GL. Microstructure and compressive properties of multicomponent $Al_x(TiVCrMnFeCoNiCu)_{100-x}$ high-entropy alloys. *Materials Science and Engineering: A*. 2007;454-455:260-265.

15. Zhou YJ, Zhang Y, Wang YL, Chen GL. Solid solution alloys of AlCoCrFeNiTix with excellent room-temperature mechanical properties. *Applied Physics Letters*. 2007;90(18):181904.

16. Hu Z, Zhan Y, Zhang G, She J, Li C. Effect of rare earth Y addition on the microstructure and mechanical properties of high entropy AlCoCrCuNiTi alloys. *Materials & Design*. 2010;31(3):1599-1602.

17. Hsu CY, Sheu TS, Yeh JW, Chen SK. Effect of iron content on wear behavior of $AlCoCrFe_xMo_{0.5}Ni$ high-entropy alloys. *Wear*. 2010;268(5-6):653-659.

18. Huang C, Zhang Z, Vilar R, Shen J. Dry sliding wear behavior of laser clad TiVCrAlSi high entropy alloy coatings on Ti–6Al–4V substrate. *Materials & Design*. 2012;41:338-343.

19. Ren B, Liu ZX, Cai B, Wang MX, Shi L. Aging behavior of a $CuCr_2Fe_2NiMn$ high-entropy alloy. *Materials & Design*. 2012;33:121-126.

20. Tsai CW, Chen YL, Tsai MH, Yeh JW, Shun TT, Chen SK. Deformation and annealing behaviors of high-entropy alloy $Al_{0.5}CoCrCuFeNi$. *Journal of Alloys and Compounds*. 2009;486(1-2):427-435.

21. Senkov NO, Wilks GB, Miracle DB, Chuang CP, Liaw PK. Refractory high-entropy alloys. *Intermetallics*. 2010;18(9):1758-1765.

22. Liu L, Zhu JB, Zhang C, Li JC, Jiang Q. Microstructure and the properties of $FeCoCuNiSn_x$ high entropy alloys. *Materials Science and Engineering: A*. 2012;548: 64-68.

23. Liu L, Zhu JB, Li L, JC Li, Jiang Q. Microstructure and tensile properties of FeMnNiCuCoSnx high entropy alloys. Mater. Des. 2013;44: 223-227.

24. Musil J, Karvánková P, Kasl J. Ward and superhard Zr-Ni-N nanocomposite films. *Surface and Coatings Technology*. 2001;139(1):101-109.

25. Uchida M, Nihira N, Mitsuo A, Toyoda K, Kubota K, Aizawa T. Friction and wear properties of CrAlN and CrVN films deposited by cathodic arc ion plating method. *Surface and Coatings Technology*. 2004;177-178:627-630.

26. Kim CW, Kim KH. Anti-oxidation properties of TiAlN film prepared by plasma-assisted chemical vapor deposition and roles of Al. *Thin Solid Films*. 1997;307(1-2):113-119.

27. Lai CH, Lin SJ, Yeh JW, Chang SY. Preparation and characterization of AlCrTaTiZr multi-element nitride coatings. *Surface and Coatings Technology*. 2006;201(6):3275-3280.

28. Tsai CW, Lai SW, Cheng KH, Tsai MH, Davison A, Tsau CH, et al. Strong amorphization of high-entropy AlBCrSiTi nitride film. *Thin Solid Films.* 2012;520(7): 2613-2618.

29. Liu L, Zhu JB, Hou C, Li JC, Jiang Q. Dense and smooth amorphous films of multicomponent FeCoNiCuVZrAl high-entropy alloy deposited by direct current magnetron sputtering. *Materials & Design*. 2013;46:675-679.

30. Zhang J, Zhu JB, Sun ZY, Li JC. Preparation of amorphous coatings of AlFeCoNiCuZrV alloy by direct current magnetron sputtering method. *Asian Journal of Chemistry*. 2014;26(17):5627-5630.

31. Chang HW, Huang PK, Davison A, Yeh JW, Tsau CH, Yang CC. Nitride films deposited from an equimolar Al–Cr–Mo–Si–Ti alloy target by reactive direct current magnetron sputtering. *Thin Solid Films*. 2008;516(16):6402-6408.

32. Huang YS, Chen L, Lui HW, Cai MH, Yeh JW. Microstructure, hardness, resistivity and thermal stability of sputtered oxide films of $AlCoCrCu_{0.5}NiFe$ high-entropy alloy. *Materials Science and Engineering: A*. 2007;457(1-2):77-83.

33. Lin MI, Tsai MH, Shen WJ, Yeh JW. Evolution of structure and properties of multi-component $(AlCrTaTiZr)O_x$ films. *Thin Solid Films*. 2010;518(10):2732-2737.

34. Inoue A. High Strength Bulk Amorphous Alloys with Low Critical Cooling Rates. *Materials Transactions JIM*. 1995;36(7):866-875.

35. Mason RS, Pichilingi M. Sputtering in a glow discharge ion source-pressure dependence: theory and experiment. *Journal of Physics D: Applied Physics*. 1994;27(11):2363.